

POLITECNICO DI TORINO

SCUOLA DI DOTTORATO

Ph.D. in [Electrical Engineering](#) – XXV cycle

A thesis submitted for the degree of
Doctor of Philosophy

**Building Integrated Photovoltaic
Systems: specific non-idealities
from solar cell to grid**



[Fabio Corona](#)

Supervisor
[Prof. Filippo Spertino](#)

Ph.D. course co-ordinator
[Prof. Mario Chiampi](#)

March 2014

I would like to dedicate this thesis to my loving family, my wife Emanuela and my beautiful daughter Elisa. I doubt this thesis would have come to fruition if it was not for them.

Acknowledgements

I would like to thank Prof. Filippo Spertino, my supervisor during all the PhD course spent in the Politecnico di Torino, for his tireless continuous support. His passion for the research on Photovoltaics is easily contagious and I own him all I learnt during this experience. I cannot forget Prof. Paolo Di Leo for his wise partnership in many works and his friendship.

I wish to thank Prof. Gianfranco Chicco as well as for his insightful discussion and collaboration. His expertise in the fields of power system and distribution system analysis, energy efficiency and power quality, allow me to improve my knowledge in the electrical engineering.

I would like to acknowledge Mr. Guido Guerra, Omnianet s.r.l. (designer and installer of the case study BIPV system), for his endless willingness, and dott. S. De Nigris and dott.ssa B. Martignoni, Province of Turin, for their constant support during the PERSIL project.

Finally, I have to acknowledge all those of the Energy Department of Politecnico di Torino, who I cannot mention here, whose help and support I always appreciated.

Contents

Contents	iii
List of Figures	vii
List of Tables	xiii
Introduction	1
1 Models for evaluating the energy performance in grid-connected in photovoltaic systems with master-slave configuration	9
1.1 Introduction to Master-Slave concept	10
1.2 Methodology of analysis	11
1.2.1 Irradiance and PV array models	15
1.2.2 Inverter model	21
1.3 Comparison for the different conditions	23
1.4 Concluding remarks	28
2 Monitoring and Checking of Performance in Photovoltaic Plants	29
2.1 PERSIL project	30
2.2 2009–2010 Radiation in Project Locations	31
2.3 Methodology of study	35
2.4 The Thirteen Monitored PV Systems	37
2.4.1 Public school “A” (9 years old)	37
2.4.2 Public school “B” (9 years old)	38
2.4.3 Public school “C” (7 years old)	38
2.4.4 Public school “D” (7 years old)	38

2.4.5	Public school “E” (8 years old)	38
2.4.6	Factory plant (4 years old)	39
2.4.7	Apartment block (3 years old)	39
2.4.8	Climbing Centre (6 years old)	39
2.4.9	Industrial Test Laboratory (3 years old)	40
2.5	Discussion about the Analysis Results	45
2.6	Concluding remarks	50
3	Solar Cell I-V Characteristics	53
3.1	Single diode model for solar cell	53
3.2	Parameters of the solar cell model	61
3.3	Parameters’ evaluation from experimental measurements	65
3.3.1	Experimental setup and measurements	65
3.3.2	Post-processing and parameter evaluation	68
4	I-V Mismatch in PV Generators	73
4.1	Series/parallel mismatch in the I-V characteristic	74
4.2	I-V mismatch on PV panel because of partial shading	75
4.3	BIPV specific non-idealities: Case Study	82
4.3.1	Large Commercial BIPV system	83
4.3.2	Technical specifications	84
4.4	I-V mismatch effect on PV array	88
4.5	I-V mismatch effect on inverter	93
4.6	Concluding remarks	96
5	Inverters for grid connection of photovoltaic systems and power quality: case studies	99
5.1	Introductory framework	99
5.2	Italian Grid Codes for HV and LV interconnections	101
5.2.1	Frequency control	105
5.2.2	Voltage stability and LVRT capability	106
5.2.3	Reactive Power capability	108
5.2.4	Active Power control	112
5.3	Methodology of the inverter analysis	112

5.4	Experimental results	114
5.4.1	3 kVA and 230 kVA inverters	114
5.4.2	Case study: shading effect on a large BIPV plant	116
5.5	Concluding remarks	119
6	Current Unbalance and Harmonic Distortion	123
6.1	Standard PQ indexes for Unbalance and Harmonic distortion . . .	124
6.1.1	Data acquisition and viewing	124
6.1.2	Experimental results	126
6.1.2.1	Variability of the power generated by the PV system	126
6.1.2.2	Assessment of the voltage and current harmonic distortions and unbalance	128
6.2	Experimental Indicators of Current Unbalance in BIPV Systems .	132
6.2.1	BIPV particularities and typologies of unbalance	132
6.2.2	Unbalance Indicators	136
6.2.2.1	Current-based components from the SC transfor- mation	137
6.2.2.2	Current components not transformed into SC . .	140
6.2.2.3	Definitions of the unbalance indicators	141
6.2.3	Experimental Results	146
6.2.3.1	Structural Unbalance	146
6.2.3.2	Unbalance from Partial Shading	148
6.2.3.3	Mixed Unbalance	156
6.2.4	Suggestions for extending the Unbalance Indicators in PQ Standards	159
6.2.5	Concluding Remarks	160
7	Conclusions	163
	Appendix A	169
	Appendix B	195
	References	215

List of Figures

1.1	Exploitation of the start-up threshold by a 3-kVA inverter.	13
1.2	Lack of advantage in master-slave configuration with respect to the centralized inverter.	14
1.3	Single centralized inverter (left); master-slave configuration with $N = 3$ inverters (right).	14
1.4	Irradiance profiles in April in Hamburg (Germany).	16
1.5	Irradiance profiles in April in Turin (Italy).	17
1.6	Irradiance profiles in April in Granada (Spain).	17
1.7	Comparison between PVGIS average irradiance profile and proposed model irradiance profile in April in Hamburg.	19
1.8	Peak values of irradiance at cloudy sky (G_d), at clear sky (G_c) and “G ratio” in Hamburg.	20
1.9	Peak values of irradiance at cloudy sky (G_d), at clear sky (G_c) and “G ratio” in Turin.	20
1.10	Fitting of the manufacturer data of an 15 kVA (type A) and 137 kVA (type B) inverters.	24
1.11	Efficiency curves function of p_{DC} referred to the rated power of SC inverter or of all the M-S inverters in simultaneous operation with $N = 3$ (best case).	24
1.12	DC-AC energy efficiency in the best case with cloudy sky and 6° tilt angle in Hamburg.	26
2.1	Locations of the 10 ARPA — Piedmont meteorological stations.	32
2.2	Solar Irradiance Data for Project Locations in 2009 and 2010 Years.	33

2.3	Details of Average Daily Solar Irradiance Data for the 4 Selected Locations.	34
2.4	Measurements vs. simulations (school A).	40
2.5	Measurements vs. simulations (school C).	41
2.6	Measurements vs. simulations (school E-2).	41
2.7	Measurements vs. simulations (industrial user-1).	42
2.8	Measurements vs. simulations (Apartment block).	42
2.9	Measurements vs. simulations (Test Lab-1).	43
2.10	Measurements vs. simulations (Test Lab-2).	43
2.11	Measurements vs. simulations (Test Lab-3).	44
2.12	Measurements of I(V) and P(V) curves at actual conditions and at STC conditions (Test Lab-2).	44
2.13	PV System Specifications and Comprehensive Performance Parameters.	46
2.14	Daily power profiles of two fixed strings.	48
2.15	Misalignment in a sun-tracker (string 3A).	49
2.16	Shading effect impact in a sun-tracker (string 3B).	49
2.17	Evolution of the shade on the climbing centre.	50
3.1	Comparison of solar spectra in winter and summer.	55
3.2	Comparison of spectral current density in winter and summer.	55
3.3	Single diode model for ideal solar cell.	56
3.4	Ideal I-V curve of a solar cell: a) as a load in two quadrants; b) as generator only in the first quadrant.	57
3.5	Effect of temperature on a solar cell I-V curve.	59
3.6	Effect of temperature on a solar cell P-V curve.	59
3.7	Effect of solar irradiance on a solar cell I-V curve.	60
3.8	Effect of solar irradiance on a solar cell P-V curve.	60
3.9	Single diode with series and parallel resistance equivalent circuit.	61
3.10	Effect of R_{sh} on a solar cell I-V curve ($R_{sh0}=17 \Omega$).	62
3.11	Effect of R_s on a solar cell I-V curve ($R_{s0}=10 \text{ m}\Omega$).	62
3.12	I-V curve measuring circuit.	66
3.13	Settings of the virtual instrument.	67

3.14 (a) Voltage (blue curve) and current (red curve) generated by the 240 W _p p-Si module during the capacitor charging. (b) Current-voltage and power-voltage curve of the 240 W _p p-Si module at experimental conditions.	67
3.15 (a) R_{s0} computation and (b) R_{sh0} and I_{SC} extrapolation.	68
3.16 I-V curves comparison.	70
4.1 I-V curves of 20 solar cell blocks in irradiated and shaded conditions.	76
4.2 I-V and P-V curves of a PV module with 1 shaded cell (model and experimental).	77
4.3 Equivalence between half shaded cell (case 1) and 20 shaded cells due to by-pass diode.	77
4.4 I-V and P-V curves of a PV module with 1/2 shaded cell, case 1 (model and experimental).	78
4.5 Equivalence between half shaded cell (case 2) and 20 shaded cells due to by-pass diode.	78
4.6 I-V and P-V curves of a PV module with 1/2 shaded cell, case 2 (model and experimental).	79
4.7 Equivalence between 2 half shaded cells and 40 shaded cells due to 2 by-pass diodes.	80
4.8 I-V and P-V curves of a PV module with two 1/2 shaded cells (model and experimental).	80
4.9 Electrical scheme of the PV system under study.	84
4.10 Geometrical layout of the PV system under study. The colours of the arrays match with the ones indicated in Fig. 4.9.	85
4.11 Particular of the partial shading over the 98 kW _p PV array no. 5 (red panels) at hour 12:15 a.m. in January.	85
4.12 Experimental results (I-V and P-V curves), on PV array no. 1 with 240 kW _p in a Spring day. Actual data and values reported to the Standard Test Conditions (STC).	86
4.13 Time evolution of the shading over the array no. 5 in the late morning of a day in July 2012 (the hours are indicated under the corresponding pair of PV modules)	89

4.14 Measurement scheme for signal acquisition on PV array no. 5 and its inverter.	89
4.15 I-V and P-V curve of array no. 5 at 11:01 in a day of July 2012. .	90
4.16 I-V and P-V curve of array no. 5 at 11:22 in a day of July 2012. .	90
4.17 I-V and P-V curve of array no. 5 at 11:54 in a day of July 2012. .	91
4.18 I-V and P-V curve of array no. 5 at 12:27 in a day of July 2012. .	91
4.19 I-V and P-V curve of array no. 5 at 12:48 in a day of July 2012. .	92
4.20 Time evolution of the P-V curves of the array no. 5 in the late morning of a day in July 2012.	92
4.21 P_{MPP} and ΔP_{MPP} vs. totally irradiated surface.	94
4.22 DC voltage and current at the inverter no. 5 input.	95
4.23 DC side inverter efficiency parameters vs. P_{MPP}	96
4.24 DC/AC efficiency of inverter no. 5 vs. P_{DC}/P_n ($P_n = 100$ kVA). .	97
5.1 Control logic of the local interface protection system for MV systems.	106
5.2 Reactive power capability ($S_n < 400$ kW).	107
5.3 Reactive power capability ($S_n \geq 400$ kW).	108
5.4 Reactive power capability ($S_n < 400$ kW).	109
5.5 Reactive power capability ($S_n \geq 400$ kW).	110
5.6 Reactive power control with power factor represented in function of P/P_n	110
5.7 Reactive power control according to $Q = f(V)$	111
5.8 Active power control in case of over-frequency.	112
5.9 Measurement scheme for 230 kVA inverter.	115
5.10 Measurement scheme for 100 kVA inverter.	115
5.11 THD of AC current and voltage for a 3 kVA inverter.	116
5.12 Amplitude of harmonic orders in terms of percentage of IAC RMS for a 3 kVA inverter.	117
5.13 THD of AC current and voltage for a phase of a 230 kVA inverter.	117
5.14 Power factor and THD_I for a 3 kVA inverter.	118
5.15 Power factor and THD_I for a 230 kVA inverter.	118
5.16 Waveforms of the three phase voltages and currents at the 100 kVA inverter output.	119

5.17	Harmonic content of the three-phase currents (100 kVA inverter).	120
5.18	Phasors of the voltages (red) and currents (black) with the positive (yellow) and negative (green) components of phase 1 current. . . .	120
6.1	The network analyser viewer.	125
6.2	Variation of the active power generated from the PV system in one week.	126
6.3	Phase voltages at the point of common coupling during the week.	127
6.4	Phase currents at the point of common coupling during the week.	127
6.5	Total Harmonic Distortion (THD) of phase voltage in one week. .	129
6.6	Total Harmonic Distortion (THD) of phase current in one week. .	130
6.7	Total Harmonic Distortion (THD) of the phase voltage in a day with partial clouding.	131
6.8	Total Harmonic Distortion (THD) of the phase voltage in a clear sky day.	132
6.9	Total Harmonic Distortion (THD) of the phase current in a day with partial clouding.	133
6.10	Total Harmonic Distortion (THD) of the phase current in a day with partial clouding.	134
6.11	Evolution of the THD_I and THD_V for the first phase, during a day in July, in clear sky conditions.	134
6.12	Evolution of the Current Unbalance Factor (CUF) and Voltage Unbalance Factor (VUF), during a day in July, in clear sky conditions.	135
6.13	Three-phase output currents of the PV system with high solar irradiance (at 16:20 in May 2013).	147
6.14	Output power for the three phases and the total PV system, with high solar irradiance and no-shading (at hour 16:20 in May 2013).	147
6.15	Unbalance indicators vs. time in case of structural unbalance. The $ITUD$ and TPU_I values are equal.	148
6.16	Time evolution of the shading over the array no. 5 in the late morning of a day in July 2012 (the hours are indicated under the corresponding pair of PV modules)	150

6.17	Time evolution of the P-V curves over the array no. 5.	151
6.18	Three-phase output currents of the array 5 inverter with partial shading (at 2 p.m. in January 2012).	154
6.19	Unbalance indicators vs. time with partial shading in the early afternoon (array no. 5). The $ITDU$ and TPU_I values are equal. .	155
6.20	Unbalance indicators vs. time with partial shading in the afternoon (array no. 4). The $ITDU$ and TPU_I values are equal.	155
6.21	Scheme of the three-phase system for signals acquisition.	157
6.22	Three-phase currents at the PCC with the PV system connected (hour 14:05 in June).	157
6.23	Three-phase currents absorbed at the PCC, without PV system (hour 14:05 in June).	159

List of Tables

1.1	Number of clear/cloudy days in the selected locations.	26
1.2	Simulated final yields in the four seasons.	27
3.1	PV module's experimental parameters.	69
3.2	Solar cell single diode model parameters at experimental conditions.	70
3.3	PV module's parameters at STC.	72
4.1	Solar Cell Parameters in Experimental Conditions.	81
4.2	Solar Cell Parameters in STC.	82
4.3	PV module's datasheet.	87
4.4	Array no.5 electrical parameters.	87
4.5	Inverter no.5 specifics.	88
4.6	P_{MPP} , P_{lim} and ΔP_{MPP} at some experimental conditions (G , T_c) and percentage of totally irradiated surface S_{irr}	93
4.7	V_{pp} , I_{pp} and η_{MPPT} for the measurements on array n. 5	95
6.1	Summary of the Unbalance Indicators.	145
6.2	Current components and Unbalance Indicators in case of structural unbalance.	149
6.3	Current components and Unbalance Indicators in case of partial shading of PV array 4.	152
6.4	Current components and Unbalance Indicators in case of partial shading of PV array 5.	153
6.5	Current components and Unbalance Indicators in case of mixed unbalance.	158

Introduction

Thesis topic

After an initial phase of great diffusion of large Photovoltaic (PV) systems installed on the ground, the recent evolution of the feed-in tariffs makes the Building Integrated PV (BIPV) systems for residential, commercial and industrial users, the more befitting application of the PV technology.

Unfortunately, the building integration implies some critical issues on the operation of principal components, such as the PV panels or the grid-connected inverter, typical of this kind of installation and not so important in the case of ground mounted PV plants. These non-idealities can be due to: presence of obstacles near the PV panels, like trees, poles, antennas, architectural elements (chimneys, barriers, buildings in the neighbourhood); non-optimal orientation of the PV field (not Southward) or with different orientations among the sub-fields, with consequent production asymmetry between morning and evening or mismatch; sub-optimal tilt angle of the PV modules, as it is fixed by the building roof; not-efficient cooling of the PV panels, which can cause temperature gradients both horizontally, between PV modules in the central area of the field and the peripheral ones, and vertically, between panels installed in the bottom and in the top of a structure, due to the direction of the cooler flow.

The consequences of these non-idealities is the subject of this PhD dissertation, from both theoretical, through convenient simulation tools, and experimental viewpoints. The most evident of these effects is the mismatch of the current-voltage characteristics of the PV field panels. With the aim of illustrating the analysis methodologies used to study the mismatch effect on all the PV system components, a specific case study is considered, constituted by a large BIPV system (almost 1MW_p) installed on the roof of a wholesale warehouse.

The theoretical study starts from the single cell encapsulated in a PV panel, completely exposed to an uniform solar irradiance. The equivalent lumped component circuit, as from the literature, is used to extract the parameters of the solar cell model, then the behaviour of single PV module subject to partial shading is reconstructed from these parameters assuming few cells with complete or partial shade. In order to obtain these results an experimental activity has been conducted on a single PV panel with different amounts and patterns of concentrated shade, in particular: with one shaded solar cell; one half shaded solar cell, with two different orientations of the shading; two solar cells, part of two different groups with its own by-pass diode, with shade on only half of them. The cell model parameters at the different irradiance conditions are extracted with numerical procedures from the experimental PV panel parameters as from the measurements. The results are new in literature since usually the cell parameters are computed only in condition of uniform irradiance on the cell surface and, when all the PV module is considered, the equivalent circuit parameters of the solar cell are calculated from the datasheet parameters of the PV panel at Standard Test Conditions (STC)¹, while in this dissertation the focus is on the cell behaviour at experimental conditions under partial shading. From the solar cell model the current-voltage characteristic of a whole block of cells in parallel with the same by-pass diode is reconstructed, so the module characteristic is computed at experimental condition under the different shading conditions. The accuracy of the simulations performed is verified comparing the experimental curve with the computed one, evaluating the RMSE ².

The study on the single PV module has been functional to the analysis of the PV arrays of the large BIPV system, subject to periodic partial shading projected by tie-beams and lateral barriers present on the triangular-shaped building roof. One of these arrays is taken as an example for illustrating the analysis methodology of the power loss assessment. An appropriate software has been used to know the shade evolution on the solar cells of each module of the sub-field considered, matching it with the distorted array current-voltage curve, measured through the capacitive charge method. Combining these measurements with the inverter

¹Solar irradiance $G=1000 \text{ W/m}^2$, Air Mass =1.5, cell temperature $T_c=25 \text{ }^\circ\text{C}$

²Root Mean Square Error

input and output voltages and currents, it has been possible to make the relation between DC power losses and inverter performance both at DC side, in terms of Maximum Power Point Tracker (MPPT) efficiency, and at AC side, in terms of DC/AC conversion efficiency.

The results have shown, as expected, a strong non-linearity between irradiated surface percentage and power at the MPP of the characteristic curves, due to the irregular deformation of the curves induced by the partial shading. This causes an inefficient tracking of the maximum power by the MPPT, adding other losses. In these conditions the inverter cannot perform the DC/AC conversion with a good efficiency, therefore on the AC side other losses are measured.

The analysis of the BIPV system from the point of view of the active user ends with the inverter and the impact of the system criticalities on the grid is considered. In particular, the consequences on the Power Quality (PQ), with reference to the unbalance and the harmonic distortion, is studied. At first the PQ indexes defined in the Standards (IEC61000-4-30, IEEE Standard 141-1993, IEC61000-4-7, EN50160, IEEE Standard 1459-2010) are used, studying the PQ degradation at low power levels, such as in the morning or in the evening. Thereafter, stressing the point that in a BIPV is always present a certain grade of unbalance due to its criticalities, other less used PQ indicators are considered, which can highlight the contribution of the harmonic distortion on the unbalance and vice versa.

These PQ indexes are for the first time applied to the study of a real case of a BIPV system and the adoption in the current PQ Standards of these indicators is suggested for the insight analysis that they allow. A classification of the unbalance is proposed, with particular reference to the three-phase currents: “structural”; “unbalance from partial shading”; “mixed unbalance”.

Thesis outline and publications

This thesis dissertation collects all the research done during the PhD course period and it is structured as outlined below.

In the chapter 1 the mathematical models for irradiance, PV array and electronic converter are defined for assessing the limits of the advisability of the master-slave configuration, in the power conversion stage of a PV system vs. a single central-

ized inverter. The simulations are performed taking into account the influence of the installation site, the PV field tilt angle, the inverter's efficiency curve and the number of slave inverters. The preliminary results were at first presented at the 26th European Photovoltaic Solar Energy Conference (conference paper n. 2), in Hamburg (Germany), then the final work was published (journal article n. 1) in the form presented in the chapter.

After this exclusively theoretical study, the chapter 2 reports the experimental campaign conducted in the framework of the PERSIL¹ project, where a two-years lasting campaign of PV systems monitoring was performed. This measurement activity on the field allows to make an assessment of the performance of various PV systems, all installed in the province of Turin, different in PV module's technology (single or poly crystalline silicon, amorphous silicon, hetero-junction, CdTe or CIS), type of installation (ground-mounted, on sun trackers, partially integrated or building integrated) and location (urban, suburbs, countryside). The PV systems were monitored according to the standard IEC 1724 [1], which defines, among other performance indicators: the *Final Yield* (Y_f), i.e., the final energy output expressed in equivalent hours; the *Reference Yield* (Y_r), i.e., the equivalent solar hours on the PV field plane; the *Performance Ratio* (R_p). The results in terms of energy monitored are compared with values of energy estimated on the basis of the Italian Standard CEI 82-25 [2] and of the meteorological data extracted from the database of the ARPA² agency of Piedmont region. The more significant experimental results were firstly presented at the 27th European Photovoltaic Solar Energy Conference (conference paper n. 4), Frankfurt (Germany), and, finally, re-processed and re-elaborated in the paper 3, where the concept of "availability" was added to assess the energy performance of a PV system.

The experience in the PV system testing, both from an energy point of view and a power standpoint, has been enriched by the study of the equivalent circuit of the PV generator. But, differently from the numerous studies present in literature, I was interested in extracting the solar cell parameters not from the PV module datasheet or measurements on a single cell in laboratory, but from measurements on a real commercial PV module on the field, as outlined in the chapter 3. This

¹Solar Performance and Local Industry (in Italian)

²Regional Agency for the Environment (in Italian)

was applied to study the behaviour of a PV module under non-ideal condition. In fact, the focus of my research shifted towards the non-idealities in the current-voltage characteristics of the PV generators, in the “other publications” n. 1 in general, and of Building Integrated PV systems in particular, since they are affected by several problems, as already highlighted in the previous section.

The chapter 4 presents the study of the consequence of the current-voltage mismatch, both theoretically and experimentally on a PV module affected by partial shading, and only experimentally on a complex PV array of the case study presented in the same chapter.

In fact, a real case study of BIPV system is illustrated. This PV plant is used as a measurement field through the whole thesis to illustrate the analysis methodology of the various elements of a PV system (i.e., array and inverter) and of some aspects of the power quality of the grid-connection (harmonic distortion and unbalance).

Therefore the chapter 5 deals with the performance of grid-connected inverters for PV systems and their power quality fed into the grid, in normal and non-ideal conditions. The contents of the chapter are extracted from the paper presented at the 3rd IEEE International Symposium on Power Electronics for Distributed Generation Systems (conference paper n. 3), in Aalborg (Denmark). The inverter studied in non-ideal conditions is one of the case study of this thesis. In the same chapter, also the new regulations for smart grid connection in presence of Distributed Generators (DG) in Italy, as written in the paper n. 2, are reviewed.

Finally, it comes the part related to Power Quality. The chapter 6 reports the studies about the BIPV system impact on the PQ of the grid-connection. The attention is focused on the harmonic distortion, the unbalance and their eventual relationship. The analysis is performed through Standard Indexes (also in the paper n. 4) and less used ones, from which detailed information is obtained, identifying the balance and unbalance components also in the presence of waveform distortion. These indices extend the current definitions of unbalance given in the power quality standards and they are applied for the first time to the study of a PV system, as far as I can know. The results of this study are currently in press (journal article n. 5). Below the list of all the publications whose I am co-author is reported.

Journal articles

1. F. Spertino, F. Corona and P. Di Leo, "Limits of Advisability for Master-Slave Configuration of DC-AC Converters in Photovoltaic Systems.", *IEEE Journal of Photovoltaics* (ISSN 2156-3381), vol. 2, n. 4, pp. 547-554, October 2012.
2. V. Barbu, G. Chicco, F. Corona and F. Spertino, "Recent Progress of the Rulemaking on Grid-Connected Photovoltaic Generation.", *Scientific Bulletin of the Electrical Engineering Faculty (Targoviste)* (ISSN 1843-6188), vol. 19, n. 2, 2012.
3. F. Spertino, P. Di Leo and F. Corona, "Monitoring and Checking of Performance in Thirteen Systems: a Tool for Design, Installation and Maintenance of Grid-Connected PV Systems", *Renewable Energy*(ISSN 0960-1481), vol. 60, pp. 722-732, 2013.
4. V. Barbu, G. Chicco, F. Corona, N. Golovanov and F. Spertino, "Impact of a Photovoltaic Plant Connected to the MV Network On Harmonic Distortion: An Experimental Assessment.", *Universitatea POLITEHNICA din Bucuresti (UPB) Scientific Bulletin, Series C* (ISSN 2286-3540), vol. 75, n. 4, pp. 179-194, 2013.
5. G. Chicco, F. Corona, R. Porumb and F. Spertino, "Experimental assessment of Unbalance and Distortion of Grid-Connected Photovoltaic Plants", *IEEE Journal of Photovoltaics* (ISSN 2156-3381), in press, doi:10.1109/JPHOTOV.2014.2307491, 2014.

Conference papers

1. F. Spertino, P. Di Leo, F. Corona and M. Montenegro, "Large/Small Scale PV Plants: Which Differences in Energy Performance and Profitability Index?", *Proc. 25th European Photovoltaic Solar Energy Conference*, 6-10 September 2010, Valencia (Spain), pp. 4664-4669.
2. F. Spertino F., P. Di Leo and F. Corona, "Energy Gains and Suitable Locations for Master-Slave Configuration of DC-AC Converters.", *Proc. 26th*

European Photovoltaic Solar Energy Conference, 5-9 September 2011, Hamburg (Germany), pp. 3721-3725.

3. F. Spertino, F. Corona, P. Di Leo and F. Papandrea, “Inverters for Grid Connection of Photovoltaic Systems and Power Quality: case studies.”, *Proc. 3rd IEEE International Symposium on Power Electronics for Distributed Generation Systems*, 25-28 June 2012, Aalborg (Denmark), pp. 564-569.
4. F. Spertino, P. Di Leo and F. Corona, “Guidelines for Design, Installation and Maintenance of PV Systems to achieve the Energy Predictions.”, *Proc. 27th European Photovoltaic Solar Energy Conference*, 24-28 September 2012, Frankfurt (Germany), pp. 4014-4019.

Other publications

1. F. Spertino, P. Di Leo P. and F. Corona, “Non-Idealities in the I-V Characteristic of the PV Generators: Manufacturing Mismatch and Shading Effect.”, *Solar Cells: Silicon Wafer-Based Technologies / L.A. Kosyachenko. Intech*, Rijeka, pp. 229-254, 2011, ISBN 9789533077475.

Chapter 1

Models for evaluating the energy performance in grid-connected in photovoltaic systems with master-slave configuration

The maximization of the productivity of a PV system is very important: this goal can be achieved by solar cell technologies with high efficiency and low temperature losses, one axis or dual axis sun-tracking systems, proper cooling techniques for PV modules in building integrated applications, master-slave control for the inverters in large grid connected PV plants, etc.. About the last item, this chapter deals with the advisability of the master-slave concept vs. the centralized inverter layout, as it has been published in [3]. Here the attention is focused on the influence of the installation site with its irradiation peculiarities, the tilt angle of the PV modules, the efficiency curve of the inverters and the number of slaves. The simulated productions put into evidence energy gains up to 4% per year, considering the only cloudy-day contribution. On the basis of these comparisons, the master-slave concept can be profitable if the number of cloudy days is sufficiently high, the tilt angle is adequate and the DC-AC efficiency curve of the inverters is “well-shaped”.

1.1 Introduction to Master-Slave concept

One of the most important aspects in an investment in a PhotoVoltaic (PV) system is the maximization of the productivity. This goal can be achieved by many solutions [4, 5], such as solar cell technologies with high efficiency and low temperature losses, one axis or dual axis sun-tracking systems, proper cooling techniques for PV modules in Building Integrated applications (BIPV) [6], power optimizers at DC side [7], Master-Slave (M-S) control for the DC-AC converter in grid connected PV plants [8, 9] etc.. Sometimes, the inverter manufacturers, when the PV power conversion is subdivided into N electronic converters, give the option to choose between the operation as multi-MPPT (Maximum Power Point Tracker) units and the operation as M-S units [10, 11]. The first solution can be more useful if partial shading problems or different orientation of the PV arrays occur: therefore, the PV field is partitioned into N arrays with matched electric parameters. On the other hand, the second solution, in which all the PV modules are arranged in a single field, supplying the equivalent resistance of the parallel-connected MPPTs, is more profitable in the cases described in the following. Obviously, the power must be shared among the inverters, according to each converter power rating and in particular divided by N , when the converters are equal sized. A different solution of load sharing is investigated in [12], where a current-decoupling control has been developed to avoid the circulating currents among the inverters operating in parallel.

With reference to equally distributed power sharing among N parallel-connected converters, this chapter is focused on the utilization of the M-S concept vs. the centralized inverter layout. From the point of view of the energy production in the framework of the feed-in tariff schemes, the M-S concept can give practical advantage when the amount of diffuse irradiation is significant in comparison with the beam component in the global radiation. In fact, the efficiency of a DC-AC converter depends on the load conditions, from zero for no-load operation to nearly 99% for optimal-load operation [13, 14]. Therefore, it is of great interest to make the DC-AC converter working close to the optimal load conditions. Usually, the power rating of a single centralized inverter matches the peak power of the PV array, thus at low irradiance levels, such as in the morning and in the

evening or with a cloudy sky, it may be more profitable to connect an inverter with reduced power rating to the same PV array, due to its improved efficiency for the same operational conditions.

Through these considerations, the M-S concept has been developed, where a Single Centralized (SC) inverter is substituted by several lower power-rating inverters, connected to the same PV generator. One DC-AC converter operates continuously as the master and the other slaves are switched on/off depending on the irradiance level, in order to maximize the global efficiency of the inverters, and therefore the energy gain.

The comparison between the “SC inverter” and the “M-S inverters” configurations is performed for different operational conditions in order to show the influence of weather and latitude of the installation site of the PV plant. In this regard, the selected countries are Germany, Italy and Spain.

The tilt angle of the PV modules is also considered in the energy gain with M-S configuration. This analysis permits to compare two different kinds of BIPV applications such as one on the roof with optimal collection or prefixed inclination and the other on a building façade.

The final aim is to obtain some general criteria for deciding when the M-S solution is a profitable option and quantifying the amount of the energy gain with respect to a single DC-AC converter. The parameters of the suitable model of DC-AC conversion efficiency and global power losses are determined by fitting manufacturer data which have been measured on inverters of different power (15–420 kVA).

1.2 Methodology of analysis

From the viewpoint of energy production, the start-up and shut-down thresholds are meaningful parameters for the Transformer-less (TL) inverters characterized by rated power $P_{inv,rated}$ ranging from a few to hundreds of kilovolt-amperes [13, 15]. These power thresholds are due to no-load consumption (internal switching and iron losses) and cooling auxiliary fan. Such a burden is close to the typical rated power of small TL inverter, with natural cooling and high efficiency down to few tens of watts.

In order to prove this concept, an extensive measurement campaign on two TL inverters, one with 230-kVA and another with 3-kVA nominal power, has been carried out.

It is worth noting that the DC-AC power signals are acquired with a suitable sampling rate (500 kSa/s), according to the switching frequency of the pulse width modulation [16, 17, 18]. In such a way, the active power takes into account the harmonic distortion impact that can worsen the energy conversion [19].

Fig. 1.1 shows that a 3-kVA inverter can use the energy that would be wasted by a 230-kVA inverter every day during sunrise and sunset periods. Its start-up threshold includes the no-load consumption, slightly less than 1 kW, and the load due to forced convection (≈ 2 kW relatively high, with respect to other commercial units, owing to undersized power switches). Moreover, it follows that other two 3-kVA inverters, in parallel with the first one at DC side, produce more energy than the single 230-kVA inverter in the range up to 10 kW. Consequently, the power of the individual inverter should be the lowest possible to minimize its start-up and shut-down thresholds. From these considerations it is argued that the PV power sharing among many inverters can give advantage in maximization of energy production. This configuration is well-known as master-slave concept [20].

On the other hand, when the PV power and also the number of parallel connected inverter become enough high, the opposite situation occurs, i.e. the 230-kVA inverter is more profitable. Fig. 1.2 illustrates the transition in terms of better efficiency from the parallel connected 3-kVA inverters (extrapolation of the efficiency curve for $N = 43$ inverters) to a single centralized 230-kVA inverter. It is clear that, at the input power level above 60 kW (nearly 25% of its rated power), the centralized inverter shows a higher efficiency.

For achieving a trade-off between the energy gain around the start-up threshold and the relatively poor efficiency at increasing load levels, the total number of inverters should be limited to few units. In general, in order to fix the total number of converters in the M-S configuration, it is necessary to find a compromise solution, in terms of energy gain, control complexity and reliability of contactors which perform the switching.

Besides the sunrise and sunset periods with daily cadence, the totally cloudy days

are characterized by input PV power under the 25% level (see in the following subsection), addressing the choice to the M-S configuration. Thus, as a first approximation criterion, the size of the single M-S inverter can be chosen around this power range at cloudy sky. In this case the master inverter can operate alone, improving the energy production with respect to the SC inverter. It is enough easy to have almost the same efficiency curve with commercial inverters if the rated power is within the ratio 5:1 [21]. Obviously, five inverters (one master and four slaves) imply higher energy gain, higher control complexity and lower reliability with respect to three converters (one master and two slaves). Here, the attention is focused on the comparison between the SC inverter (Fig. 1.3 on the left) and the M-S configuration with $N = 3, 4$ or 5 inverters, all connected in parallel (Fig. 1.3 on the right).

The master inverter controls the activation of the other converters by means of contactors, in order to obtain the highest value of the DC-AC conversion efficiency in each moment of the day for each value of DC input power. Therefore, first of all, it is necessary to fix the same DC input power for the two solutions. The basic “impact factor” for the comparison is the irradiance profile subject to the weather fluctuations.

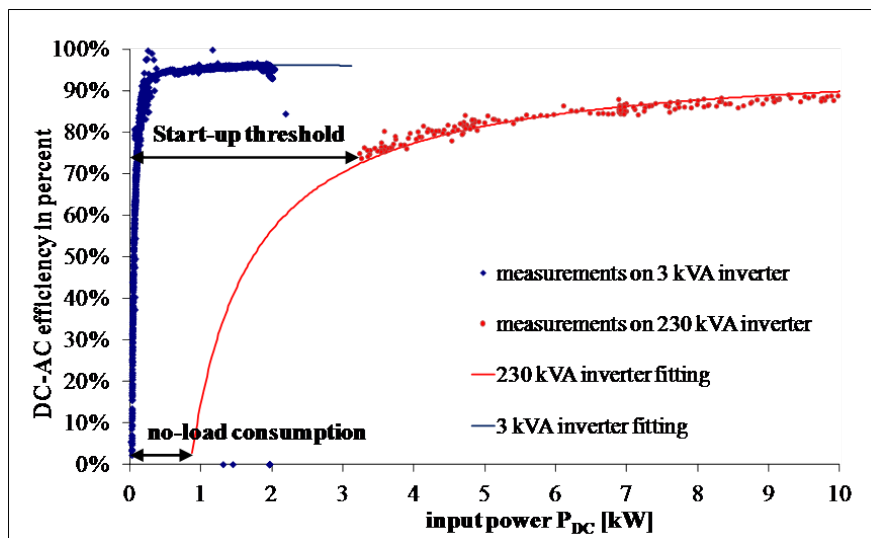


Figure 1.1: Exploitation of the start-up threshold by a 3-kVA inverter.

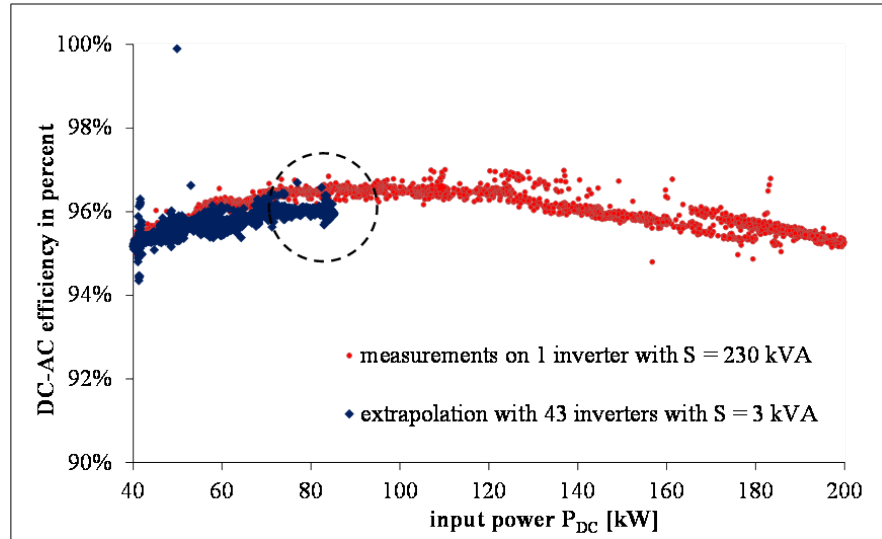


Figure 1.2: Lack of advantage in master-slave configuration with respect to the centralized inverter.

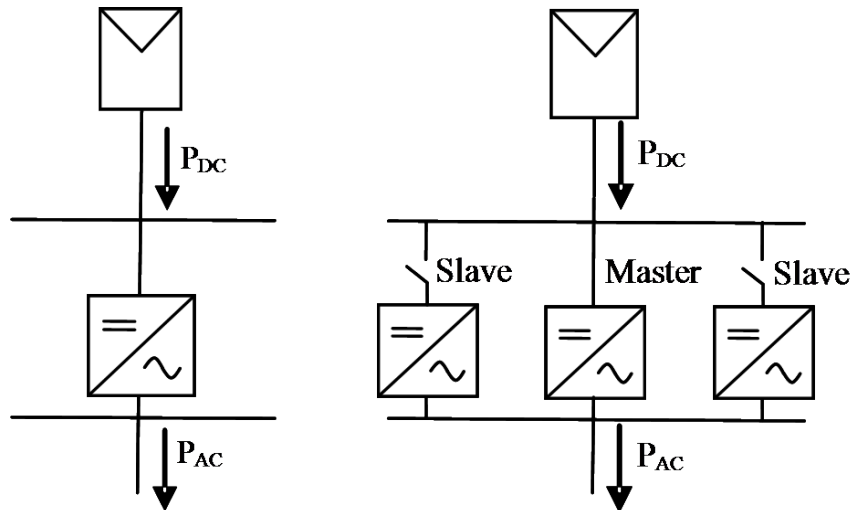


Figure 1.3: Single centralized inverter (left); master-slave configuration with $N = 3$ inverters (right).

1.2.1 Irradiance and PV array models

Two opposite weather conditions have been considered: totally cloudy and clear sky days. That is, in cloudy conditions it is expected the maximum advantage for the M-S configuration vs. a SC inverter, while at clear sky it is the opposite. The irradiance (G) profiles for both atmospheric conditions are extracted for suitable locations at different latitude: Hamburg (Germany) at latitude 53° North, Turin (Italy) at 45° N and Granada (Spain) at 37° N. In particular, Hamburg represents the most unfavourable site, in terms of number of clear-sky days, Turin is an intermediate location, close to Southern Germany and Northern Spain, finally Granada represents the best site, roughly similar to Southern Italy.

For each PV-generator installation site and sky condition, twelve daily irradiance profiles, each one representative of the average behaviour of a different month, are taken into account to have the yearly trend for each location. The tilt angle β of the PV array is set by the kind of application. The tilt angle, optimal from the yearly-energy point of view, is chosen if the PV modules are placed at the ground level or on a flat roof (33° – 38°), while its value is constrained if the PV modules are mounted on a façade (90°) or on a tilted roof (6° for an industrial shed and 30° for residential roof).

Practical irradiance profiles for both the weather conditions have been processed from the meteorological database of the Joint Research Centre of the European Commission (PVGIS), with reference to the three locations [22]. Here three examples of G profile, corresponding to the best tilt angle, in a mean day of April, are reported for Hamburg (Fig. 1.4), Turin (Fig. 1.5) and Granada (Fig. 1.6).

The diffuse component of the global irradiance at real sky is taken as representative of the cloudy sky irradiance. The models of three types of day are used, in which the clear sky waveform is represented with a red curve (G_c), the cloudy sky one with a green curve (G_d) and the real sky one with a blue curve (G). The real-sky profile of the irradiance is an average among all the month days, for each time interval, and, consequently, it has not a meaning in terms of practical daily pattern. Hence, due to the non-linearity of the energy conversion in the PV modules and inverters (as illustrated in the following), simulations consider

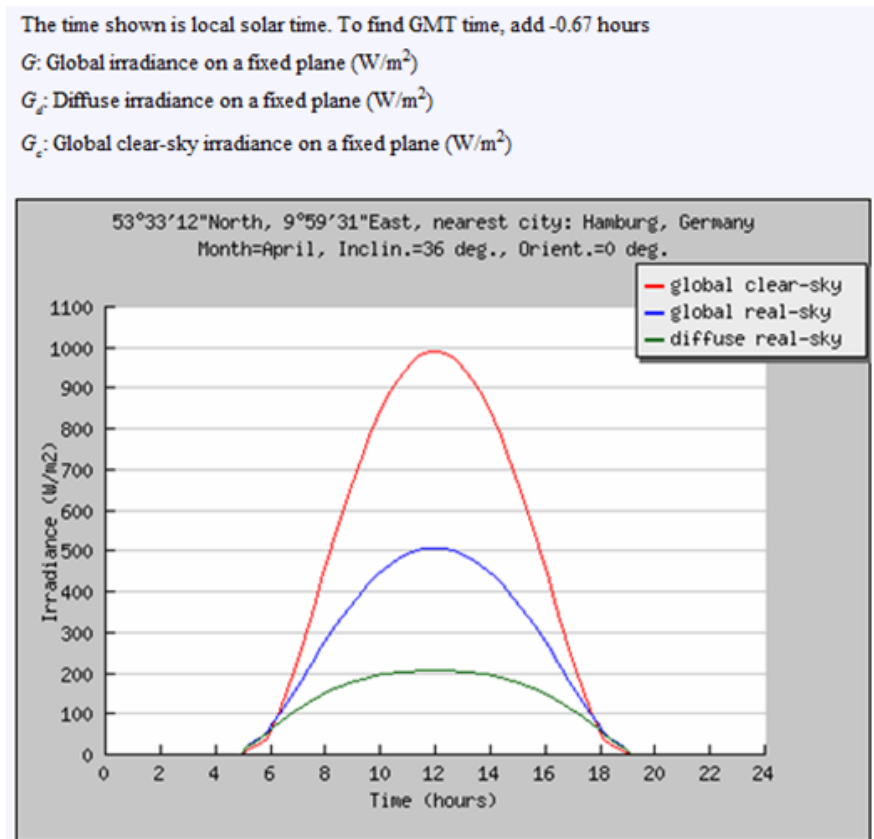


Figure 1.4: Irradiance profiles in April in Hamburg (Germany).

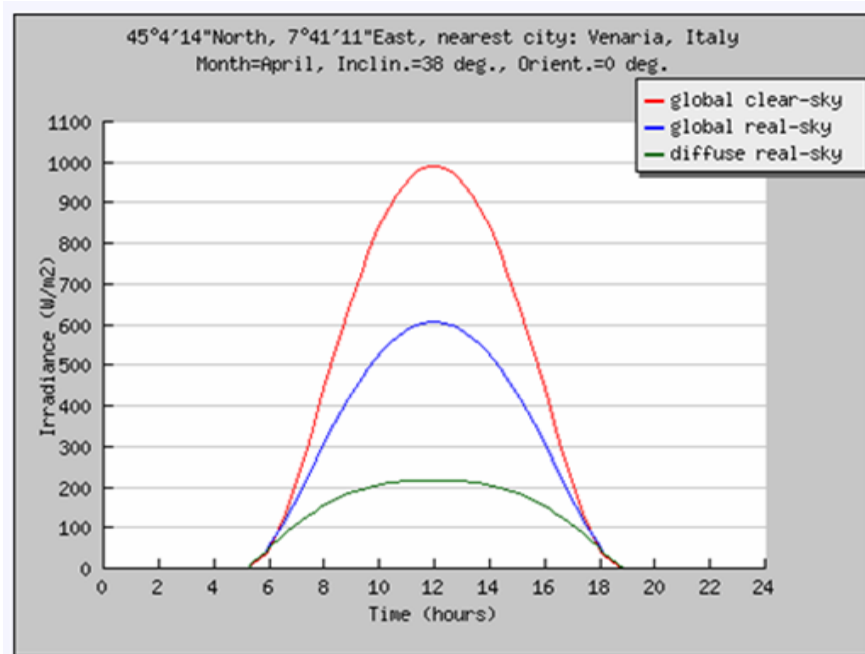


Figure 1.5: Irradiance profiles in April in Turin (Italy).

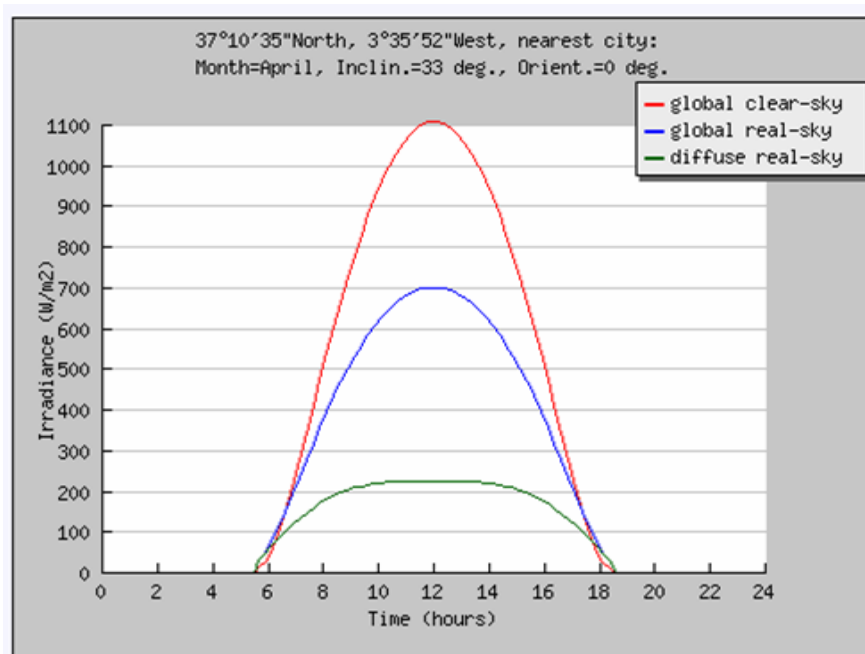


Figure 1.6: Irradiance profiles in April in Granada (Spain).

a month as a weighted combination of clear days N_c and cloudy days N_d . Thus, the monthly irradiation for the energy estimation can be obtained by the following proposed formula, rather than considering the global real-sky waveform (G_k) multiplied by the total number of days in the month (N_m):

$$H_m = N_m \cdot \Delta t \cdot \sum_k G_k \approx N_c \cdot \Delta t \cdot \sum_k G_{ck} + N_d \cdot \Delta t \cdot \sum_k G_{dk} \quad (1.1)$$

where Δt is a quarter of hour, G_{ck} and G_{dk} are the mean value of “direct + diffuse” and “diffuse alone” irradiance, respectively, in every quarter of hour, corresponding to clear and cloudy days. “Broken-clouds” situations (abrupt variations from clear to cloudy sky and vice versa in the same day) are, necessarily, included partly into clear sky days and partly into cloudy sky days. Checking this approach with the least square error method, satisfactory results have been achieved.

Actually, the deviations between the PVGIS real-sky waveform and the reconstructed profile are below 50 W/m^2 in every case (Fig. 1.7). As per the monthly irradiation, a site is better than another one if, with the same clear sky and cloudy sky waveforms, the real sky waveform is higher than the corresponding waveform of the other one (more N_c days). An example of this situation can be found when the cities of Hamburg and Turin (the sunnier), characterised by different latitude, are examined (Figs. 1.4–1.5).

It is important to define the “G ratio” of the peak values (at local noon) of clear sky irradiance to the cloudy sky one. This parameter can roughly fix the number of inverters which share the maximum load with the highest irradiance in the M-S configuration. Considering the best tilt angle, the “G ratio” is in the range 4–9 in Hamburg (Fig. 1.8), 4–6 in Turin (Fig. 1.9) and in Granada. The power inputs of the DC-AC converters are calculated from the irradiance profile [23, 24, 25]. The DC power in the MPP of the current-voltage (I-V) characteristic is supposed proportional to the irradiance through the ratio $P_{PV,peak}/G_{STC}$. Together with $G_{STC} = 1000 \text{ W/m}^2$, the temperature $T_{STC} = 25 \text{ }^\circ\text{C}$ defines the Standard Test Conditions (STC) at which the “peak” (rated) power $P_{PV,peak}$ is measured for all the commercial PV modules. The MPP Tracker efficiency is set to 99% and the losses due to reflection, DC cables, dirt, tolerance and I-V curves mismatch are

globally supposed equal to 8% [2]. The over-temperature losses (with respect to STC) are calculated by

$$k_T = \gamma_T \cdot (T_c - T_{STC}) \quad (1.2)$$

where γ_T is the thermal coefficient of power of the modules, dependent on the PV technology (for silicon $\gamma_T \approx -0.5 \text{ \%}/^\circ\text{C}$), and T_c is the solar cell temperature. This temperature is estimated with a linear combination of the ambient temperature T_a and the irradiance G on the PV plane by a parameter which provides its influence ($^\circ\text{C m}^2 \text{ W}^{-1}$). The formula 1.3 yields the input DC power:

$$P_{DC} = P_{PV,peak} \cdot \frac{G}{G_{STC}} \cdot (1 - 0.08 - 0.01 - k_T) \quad (1.3)$$

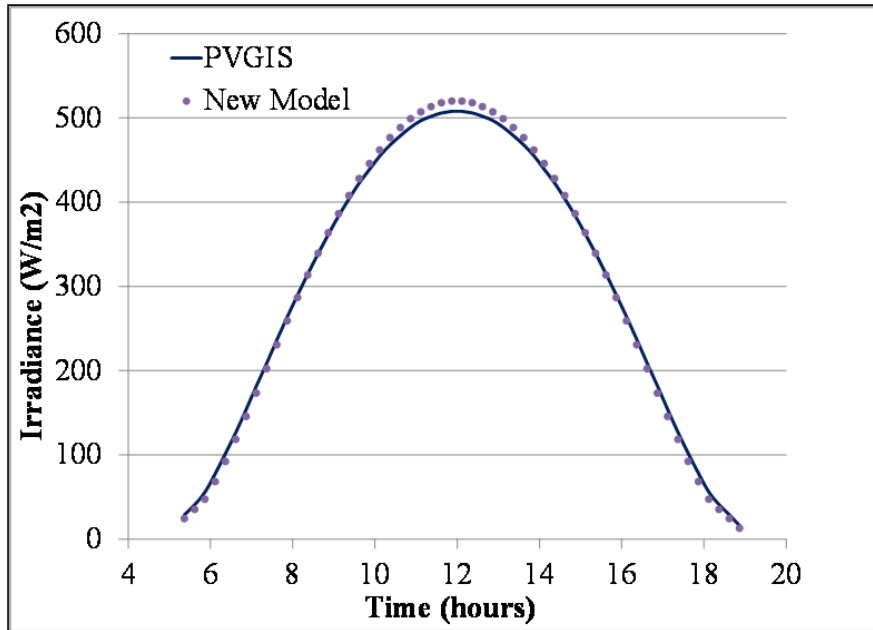


Figure 1.7: Comparison between PVGIS average irradiance profile and proposed model irradiance profile in April in Hamburg.

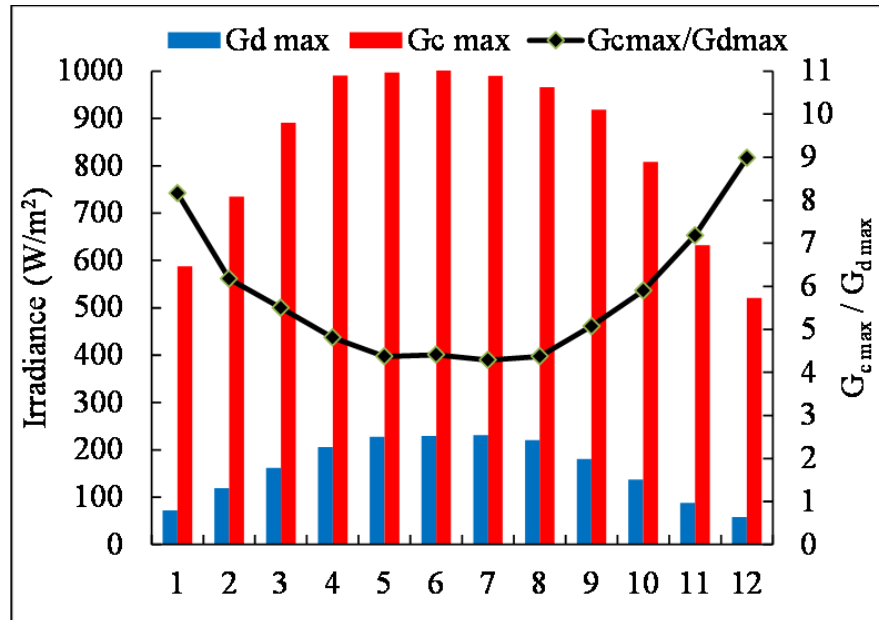


Figure 1.8: Peak values of irradiance at cloudy sky (G_d), at clear sky (G_c) and "G ratio" in Hamburg.

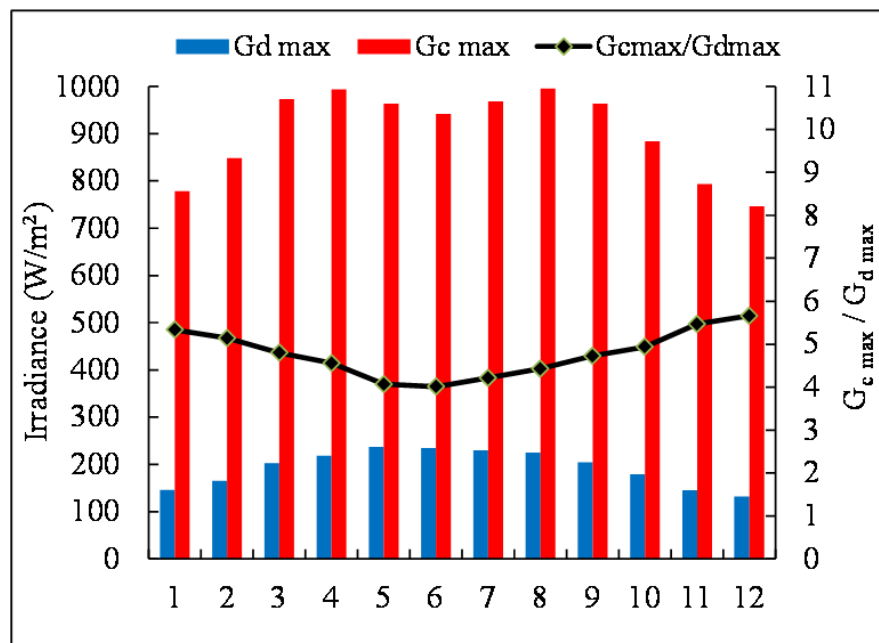


Figure 1.9: Peak values of irradiance at cloudy sky (G_d), at clear sky (G_c) and "G ratio" in Turin.

1.2.2 Inverter model

The power outputs of the inverters are calculated from the DC power input, taking into account the DC-AC power conversion efficiency. By examining a TL inverter structure, the DC-AC conversion efficiency is defined as the ratio of the AC power delivered to the grid, P_{AC} , to the DC input power P_{DC}

$$\eta_{inv} = \frac{P_{AC}}{P_{DC}} = \frac{P_{AC}}{P_{AC} + P_{loss}^{glob}} \quad (1.4)$$

where P_{loss}^{glob} are the global losses of the converter, defined as [26]

$$P_{loss}^{glob} = P_0 + c_L \cdot P_{AC} + c_S \cdot P_{AC}^2 \quad (1.5)$$

with the following meaning

P_0 are the no-load power losses along the operation (due to the supply of auxiliary circuits);

c_L is the linear loss coefficient (due to the conduction of diodes, IGBT transistors and switching losses);

c_S is the square loss coefficient (due to the conduction of MOSFET transistors and the resistive contribution).

Thus, by using the solving formula of the 2nd order equation, P_{AC} is calculated from the input power and the loss parameters of the inverter model as follows

$$P_{AC} = \frac{-(1 + c_L) + \sqrt{(1 + c_L)^2 + 4 \cdot c_S \cdot (P_{DC} - P_0)}}{2 \cdot c_S} \quad (1.6)$$

for $P_{AC} < P_{inv,rated}$ and equal to zero if greater than the nominal power of the inverter, which is assumed coincident with $P_{PV,peak}$. Towards an easy comparison of solutions, the ratios “power input and power output to the inverter power rating” $P_{DC}/P_{inv,rated}$ and $P_{AC}/P_{inv,rated}$ can be determined. These are named supply and load factors p_{DC} and p_{AC} in per unit, from which the normalized loss

parameters are defined:

$$\dot{P}_0 = \frac{P_0}{P_{inv,rated}}; \quad \dot{c}_L = c_L; \quad \dot{c}_S = c_S \cdot P_{inv,rated} \quad (1.7)$$

Then, the DC-AC conversion efficiency and the normalized AC power can be expressed by

$$\eta_{inv}(p_{AC}) = \frac{p_{AC}}{p_{DC}} = \frac{p_{AC}}{p_{AC} + \left(\dot{P}_0 + \dot{c}_L \cdot p_{AC} + \dot{c}_S \cdot p_{AC}^2 \right)} \quad (1.8)$$

$$p_{AC} = \frac{-(1 + \dot{c}_L) + \sqrt{(1 + \dot{c}_L)^2 + 4 \cdot \dot{c}_S \cdot (p_{DC} - \dot{P}_0)}}{2 \cdot \dot{c}_S} \quad (1.9)$$

The loss parameters have been determined by fitting, with the least square method, the manufacturer data of TL inverters of different size: 15, 137 and 422 kVA, named as types A, B and C [21]. Fig. 1.10 shows the fitting for the first two inverter types, while the efficiency curve of the highest power class (type C) is omitted because almost coincident with the second class one (type B). The interpolation is generally very good, except for two points at $p_{AC} = 0.1$ with a 0.007 efficiency deviation in type A and at $p_{AC} = 0.25$ with a 0.005 efficiency deviation in type B. However, by using a piecewise fitting of the data sheet's points (MATLAB environment [27]) the impact of this deviation determines a negligible error of 0.11%–0.13% in the yearly energy. Looking at the interpolated curves, the efficiency of the type A is higher than the type B at both low ($0 \div 0.05$) and full load factor ($0.9 \div 1$). Indeed, the no-load power losses and the square loss coefficient are lower, while the linear loss coefficient is higher, determining a worse performance of type A in the mid-power range.

In order to compare the global efficiency of the M-S configuration with the SC solution, two cases are examined: the best and the worst case. As common basis in the two cases, the rated power of every inverter operating in M-S configuration is equal to $1/N$ of the SC-solution's rated power. In the M-S configuration let us assume that the supply and load factors p_{DC} and p_{AC} are calculated taking into account the number of inverters simultaneously operating. It can be summarized by the 1.10 and 1.11 equations of p_{DC} and p_{AC} , with respect to SC solution, for the determination of global efficiency in M-S configuration with “n of N” inverters

in operation:

- one inverter in operation

$$p_{DC}^{1-inv} = N \cdot p_{DC}^{SC}; \quad p_{AC}^{1-inv} = N \cdot p_{AC}^{SC} \quad (1.10)$$

- n inverters in operation

$$p_{DC}^{n-inv} = \frac{N}{n} \cdot p_{DC}^{SC}; \quad p_{AC}^{n-inv} = \frac{N}{n} \cdot p_{AC}^{SC} \quad (1.11)$$

In the worst case the DC-AC efficiency curve of the SC inverter (type B) is higher than the curve of all the M-S inverters in simultaneous operation (type A) above $p_{AC} = 0.05$ and below $p_{AC} = 0.9$, as already said. In the best case, the DC-AC efficiency curve of all the M-S inverters in simultaneous operation (type B) is higher than the SC curve (type C). It can be pointed out that in the worst case these three inequalities are valid

$$\dot{P}_0^{N-inv}(A) < \dot{P}_0(B), \dot{c}_L^{N-inv}(A) > \dot{c}_L(B), \dot{c}_S^{N-inv}(A) < \dot{c}_S(B)$$

The global efficiency is given by the overlapping of the master inverter and of the added slaves. With reference to the best case, the efficiency curves of the SC and the M-S configurations with the start-up thresholds of 1-2 slaves ($p_{AC} \approx 0.19$ and $p_{AC} \approx 0.33$) are shown in Fig. 1.11.

1.3 Comparison for the different conditions

At the aim of covering multiple case studies of master-slave application, the simulation results, concerning crystalline silicon PV modules, are referred to:

- different locations in terms of latitude, “G ratio” and number of cloudy/clear days per year;
- different tilt angles of PV modules from very low slope (industrial building) to 90° façade;

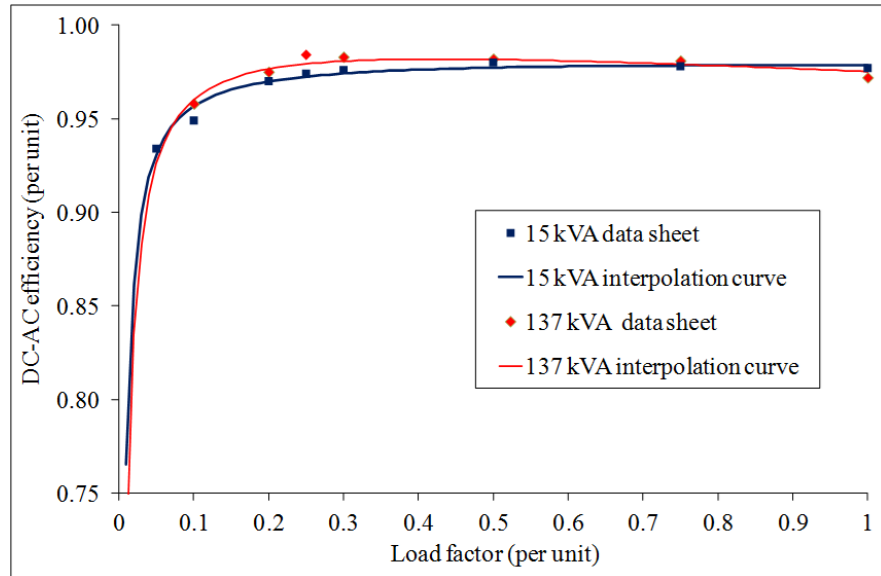


Figure 1.10: Fitting of the manufacturer data of an 15 kVA (type A) and 137 kVA (type B) inverters.

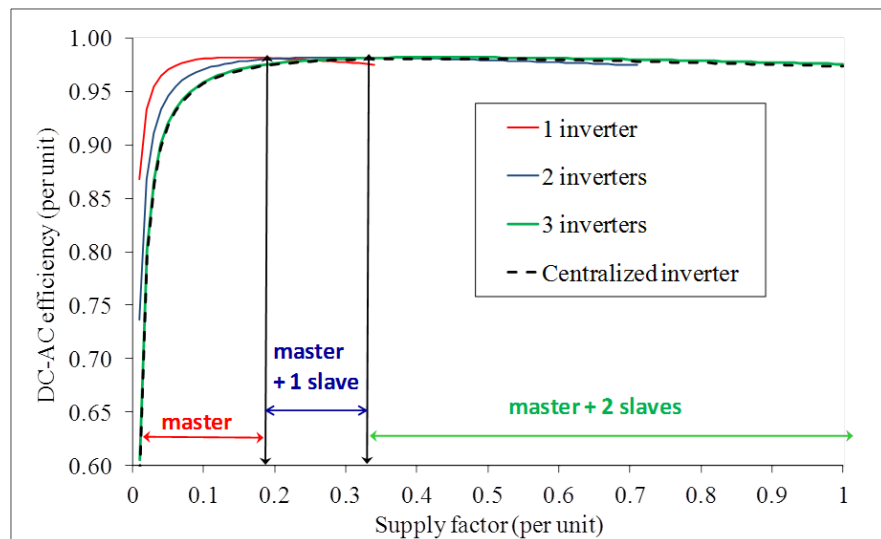


Figure 1.11: Efficiency curves function of p_{DC} referred to the rated power of SC inverter or of all the M-S inverters in simultaneous operation with $N = 3$ (best case).

- different efficiency curves of the SC inverter and of the M-S inverters (type A, B, C);
- different number of M-S inverters ($N = 3$ to 5).

Both the best tilted roof on yearly basis (36° for Hamburg, 38° for Turin and 33° for Granada [28]), the typical roof of industrial buildings (6° slope) and the 90° angle façade are considered with South orientation. PV systems of different configurations and at different locations can be readily compared by evaluating their normalized performance indices such as yields and efficiencies. Yields are energy quantities normalized to rated array power $P_{PV,peak}$ [29]. The final yield Y_f is the portion of the daily energy output of the entire PV plant which is supplied by the array per kilowatt of power. This yield represents the number of hours per day that the array would need to operate at its rated power $P_{PV,peak}$ to equal its measured energy.

The number of clear days vs. cloudy days is shown in Table 1.1, in which it can be noted that in Hamburg nearly 70% of the total number is constituted by cloudy days, making it the most convenient location, due to the high impact of diffuse radiation in the global one. The opposite situation occurs in the other two cities: 40%–45% of the days represents cloudy days.

In regards to Hamburg, with the minimum tilt angle and a remarkable gain, the main findings by MATLAB are presented in the following. The best months are January and December, which have both the maximum “G ratio” and the maximum number of cloudy days. With cloudy sky conditions, for the best case, the M-S configuration with 5 inverters achieves gain up to 15%. The DC-AC energy efficiencies are reported in Fig. 1.12, where the energy gains of the 4 or 5 M-S inverters are practically vanishing from March to October with respect to the 3 M-S inverter configuration. The annual gain of M-S configurations in the energy is within 0.4–1.5% range, according to the various tilt angles, efficiency curve types and number of M-S inverters (Table 1.2, where the best figure is on façade). Limiting the analysis to the optimal tilt angle, in Turin the yearly gain of M-S configurations is within 0.3–0.75% range, while in Granada the corresponding gain is within 0.1–0.3% range: these results demonstrate no practical advantage in Southern Europe for M-S configuration (Table 1.2).

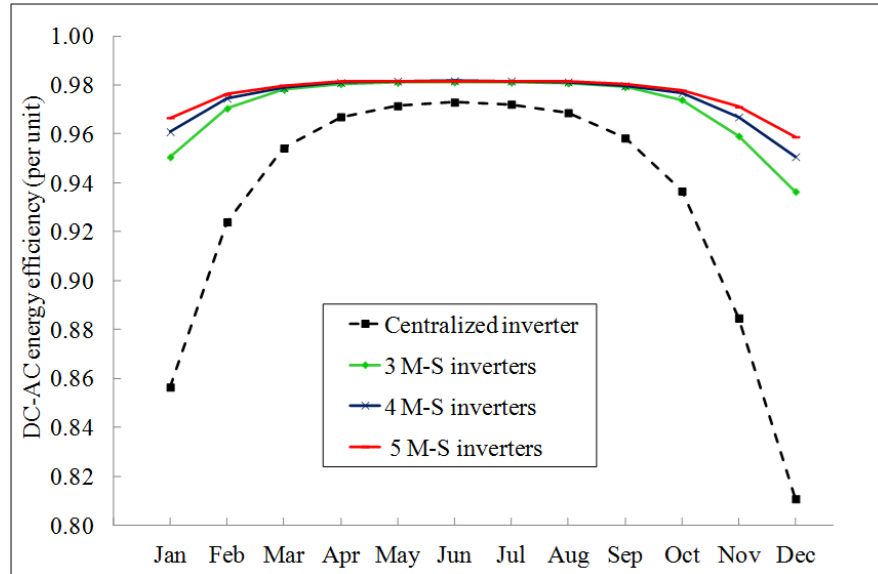


Figure 1.12: DC-AC energy efficiency in the best case with cloudy sky and 6° tilt angle in Hamburg.

Hamburg					
Season	Winter	Spring	Summer	Autumn	Year
Clear Days	18	35	35	27	115
Cloudy Days	72	57	57	64	250

Turin					
Season	Winter	Spring	Summer	Autumn	Year
Clear Days	42	47	61	50	200
Cloudy Days	48	45	31	41	165

Granada					
Season	Winter	Spring	Summer	Autumn	Year
Clear Days	46	54	66	52	218
Cloudy Days	44	38	26	39	147

Table 1.1: Number of clear/cloudy days in the selected locations.

Hamburg, tilt 6°, best case		Winter	Spring	Summer	Autumn	Gain
SC	[kWh/kW]	61	290	343	139	-
3 inv. M-S	[kWh/kW]	64	292	344	142	1.19%
4 inv. M-S	[kWh/kW]	64	292	345	142	1.27%
5 inv. M-S	[kWh/kW]	64	292	345	143	1.32%
Hamburg, tilt 6°, worst case		Winter	Spring	Summer	Autumn	Gain
SC	[kWh/kW]	61	290	343	140	-
3 inv. M-S	[kWh/kW]	64	291	343	142	0.70%
4 inv. M-S	[kWh/kW]	64	291	344	142	0.81%
5 inv. M-S	[kWh/kW]	64	291	344	142	0.85%
Hamburg, tilt 36°, best case		Winter	Spring	Summer	Autumn	Gain
SC	[kWh/kW]	91	315	349	180	-
3 inv. M-S	[kWh/kW]	93	317	351	182	0.86%
4 inv. M-S	[kWh/kW]	93	317	351	182	0.91%
5 inv. M-S	[kWh/kW]	93	318	351	182	0.93%
Hamburg, tilt 90°, best case		Winter	Spring	Summer	Autumn	Gain
SC	[kWh/kW]	89	210	197	157	-
3 inv. M-S	[kWh/kW]	90	212	199	159	1.34%
4 inv. M-S	[kWh/kW]	91	213	200	159	1.43%
5 inv. M-S	[kWh/kW]	91	213	200	159	1.47%
Turin, tilt 38°, best case		Winter	Spring	Summer	Autumn	Gain
SC	[kWh/kW]	216	362	421	292	-
3 inv. M-S	[kWh/kW]	218	364	423	294	0.60%
4 inv. M-S	[kWh/kW]	218	364	423	294	0.73%
5 inv. M-S	[kWh/kW]	218	364	423	294	0.75%
Granada, tilt 33°, best case		Winter	Spring	Summer	Autumn	Gain
SC	[kWh/kW]	309	426	444	355	-
3 inv. M-S	[kWh/kW]	310	428	446	357	0.43%
4 inv. M-S	[kWh/kW]	310	428	446	357	0.44%
5 inv. M-S	[kWh/kW]	310	428	446	357	0.45%

Table 1.2: Simulated final yields in the four seasons.

1.4 Concluding remarks

In order to evaluate the option of the master-slave concept with respect to the single centralized inverter, here the attention has been focused on the influence of the installation site, the tilt angle of the PV modules, the DC-AC efficiency curves of commercial inverters and the number of slaves. The tables, which resume the simulated energies, put into evidence annual gains in the range 0.1–1.5%, according to the various locations.

Therefore, the M-S configuration is advisable in sites with more cloudy days than clear days: the best applications are on nearly flat roofs (higher diffuse radiation) and façades (lower direct radiation). Moreover, the DC-AC efficiency of M-S inverters must not be lower than the SC inverter.

Then, the number of M-S inverters can be limited to 3 for achieving almost the maximum gain. Regarding the costs, the manufacturers usually offer M-S and multiple MPPT units as alternative options, so the M-S solution does not imply extra-cost for installation. Moreover, the single inverters are units which exchange their role as master/slave and they are not exploited continuously, but the operation is controlled for tracking the working points with maximum efficiency. This reduces the working time of each unit (i.e. the maintenance cost) and it assures an higher expected lifetime. Finally, the Master-Slave solution is therefore advisable with the application limits highlighted in this chapter.